JOURNAL OF GEOPHYSICAL RESEARCH, VOL. 106, NO. D10, PAGES 10,289–10,297, MAY 27, 2001

Wavelet analysis of stratospheric gravity wave packets over Macquarie Island 2. Intermittency and mean-flow accelerations

Florian Zink and Robert A. Vincent
Department of Physics and Mathematical Physics, University of Adelaide, Adelaide, South Australia

Abstract. We calculate the mean-flow accelerations due to gravity wave packets observed in the lower stratosphere over Macquarie Island (55°S, 159°E) between February 1994 and April 1995. The parameters of the wave packets were extracted from twice-daily radiosonde soundings using a wavelet-based analysis method introduced by *Zink and Vincent* [this issue]. The deduced wave parameters are used to directly compute momentum flux profiles in the lower stratosphere, and the shortcomings of this approach to assess mean-flow accelerations are discussed. We then use the observed wave packets as an input spectrum in a linear ray-tracing model. The vertical extent of the detected wave packets allows us to define an expression for wave intermittency, which enables us to compute zonal accelerations in the stratosphere and mesosphere. In the stratosphere the waves produce an acceleration of the mean flow, in accordance with predictions. In the mesosphere the inferred wave drag is 2-3 times larger than previous observational and theoretical estimates.

1. Introduction

Gravity waves can transport energy and momentum from the troposphere to the middle and upper atmosphere (see *Fritts* [1984] for a review) and influence large-scale temperature and circulation patterns [*Geller*, 1983]. Using the gravity wave parametrization of *Lindzen* [1981], the importance of wave drag and diffusion in the middle atmosphere was demonstrated in numerical simulations [*Holton*, 1982, 1983; *Dunkerton*, 1982; *Garcia and Solomon*, 1985]. For low-frequency gravity waves, both the vertical flux of horizontal momentum and the horizontal transport of heat are important to describe the wave mean-flow interactions. Both contributions are contained in the so-called Eliassen-Palm flux, which can be expressed as $\rho\overline{u'w'}\delta_-$, where $\delta_- = 1 - f^2/\omega^2$ [*Fritts and Vincent*, 1987]. The resulting zonal acceleration of the mean background flow can then be expressed as

$$\langle A_{\text{zonal}} \rangle = -\frac{1}{\rho}\frac{\partial}{\partial z}\langle \rho\overline{u'w'}\delta_- \rangle, \qquad (1)$$

where strictly the angle brackets should be a zonal average, but here they denote a temporal average [*Fritts and Vincent*, 1987]. Profiles of momentum flux can either be computed directly from measurements at the respective height levels, or they can be inferred from modeling studies where a given gravity wave source spectrum is propagated through the atmosphere.

In a companion paper [*Zink and Vincent*, this issue] hereinafter referred to as ZV, we introduced an analysis technique to detect gravity wave packets in high-resolution radiosonde soundings. Wave packets in horizontal wind velocity were detected using the wavelet transform and the wave parameters extracted by Stokes parameter analysis. Here the vertical extent of the packet is defined as the fullwidth at half maximum of the horizontal wind variance of the reconstructed wave packet. The packet is reconstructed by summing the complex coefficients of all attributing wavelets (see ZV for further details).

Application of the technique to twice-daily soundings at Macquarie Island (55°S, 159°E) for a period of 2 years allowed us to deduce the characteristics of gravity wave packets in the lower stratosphere. Parameters such as horizontal and vertical wavenumbers, intrinsic frequency, packet amplitude, and vertical extension were computed for wave packets observed in the height region between 15 and 30 km for summer (November to March) and winter (April to October). These parameters are important to initialize gravity wave parametrization schemes [*Lindzen*, 1981; *Fritts and VanZandt*, 1993; *Hines*, 1997; *Warner and McIntyre*, 1999], which are used in numerical models to take unresolved wave effects into account. In our discussion, special emphasis was put on the observational filter

Paper number 2000JD900846.
0148-0227/01/2000JD900846$09.00

inherent in our radiosonde measurements [*Alexander*, 1998]. The method can only observe waves with vertical wavelengths between ~1.2 and 11 km. Waves with wavelengths outside this region are either strongly attenuated by smoothing inherent in the radiosonde data processing or they are difficult to distinguish from variations in the background atmosphere.

In this paper we use the inferred parameters to assess the effect the observed waves have on the mean flow in the lower and middle atmosphere. As the signal-processing parameters of the radiosonde equipment were altered in January 1994, only soundings after that date were included in our analysis. In section 2 we compute the momentum flux profile from the gravity wave parameters of each observed wave packet and discuss the shortcomings of such profiles for the assessment of wave mean-flow interactions. To overcome some of these problems, we derive an expression for wave intermittency in section 3 and apply it to deduce the effects of the observed gravity waves on the background atmosphere in a linear ray-tracing model. We conclude the paper with a summary in section 4. Notations and gravity wave polarisation and dispersion relations are the same as applied in ZV.

2. Calculation of Momentum Flux Profiles

Different observational techniques have been used to estimate momentum fluxes in the lower atmosphere. *Lilly and Kennedy* [1973] and *Alexander and Pfister* [1995] used aircraft-mounted systems to measure momentum fluxes associated with orographically and convectively generated gravity waves, respectively. *Vincent and Reid* [1983] developed a radar method to infer momentum fluxes from symmetric-beam Doppler measurements, which has been applied in the lower and middle atmosphere [*Fritts et al.*, 1990; *Sato*, 1994; *Murayama et al.*, 1994; *Worthington and Thomas*, 1996; *Reid and Vincent*, 1987; *Tsuda et al.*, 1990].

Radiosonde data have also been used for estimation of momentum fluxes. *Shutts et al.* [1988] calculated the momentum flux of a single gravity wave from fluctuations in balloon ascent rate and horizontal perturbation velocities. *Mobbs and Rees* [1989] made use of the same variables to compute momentum flux profiles over the whole sounding range. The estimation of the vertical perturbation velocity from fluctuations in balloon ascent rate, however, is only reliable for large-amplitude waves. Smaller fluctuations can be due to measurement errors of radiosonde altitude or changed drag coefficients of the balloon.

It can therefore be advantageous to calculate the vertical perturbation velocity from observed temperature fluctuations, which are measurable with a much higher accuracy. If the intrinsic frequency of the contributing waves is known, the momentum flux can be expressed using the polarization relations as

$$\overline{\rho u' w'} = -\rho \frac{\hat{\omega} g}{N^2} \overline{u' \hat{T}'_{+90}}. \quad (2)$$

Here the overbar denotes spatial average and $\hat{T}'_{+90}$ is the vertically 90° phase-shifted (i.e., Hilbert transformed), normalized temperature fluctuation $\hat{T}'$ so that $u'\hat{T}'_{+90}$ changes sign according to the sign of m.

Sato and Dunkerton [1997] analyzed 10 years of twice-daily radiosonde data at Singapore. They calculated quadrature spectra from time series of horizontal wind speeds and temperature and used (2) to compute the corresponding momentum fluxes. They ignored the Doppler shift between intrinsic and ground-based frequency and used the ground-based frequency in their computations, since the mean wind in the considered height range was weak. *Vincent et al.* [1997] and *Allen* [1996] fitted observed mean spectra to the spectral parameterization of *Fritts and VanZandt* [1993] and integrated over the model spectrum to find an intrinsic mean frequency $\overline{\hat{\omega}}$, which was then used in (2) to compute the momentum flux from measured values of $\overline{u'\hat{T}'_{+90}}$. Their method therefore assumes similar propagation characteristics for all waves independent of frequency, even though mainly low-frequency waves were resolved.

The wavelet analysis developed in ZV provides all required gravity wave parameters to compute the momen-

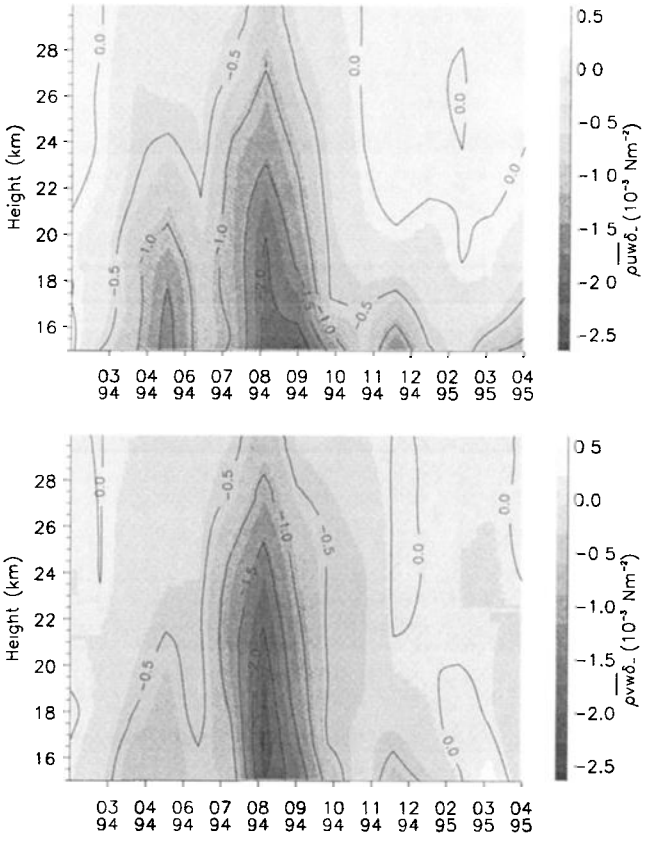

Figure 1. Contour plots of monthly averages of momentum fluxes (top) $\overline{\rho u' w' \delta_-}$ and (bottom) $\overline{\rho v' w' \delta_-}$ for waves with intrinsic frequencies less than 10 f.

Table 1. Mean values of Momentum Fluxes for Winter and Summer at Heights of 20 and 28 km

	$\langle\overline{u'w'}\delta_-\rangle$, m^2s^{-2}	$\langle\overline{v'w'}\delta_-\rangle$, m^2s^{-2}	$\langle\rho\overline{u'w'}\delta_-\rangle$, Nm^{-2}	$\langle\rho\overline{v'w'}\delta_-\rangle$, Nm^{-2}
Winter, 20 km	-1.3×10^{-2}	-1.2×10^{-2}	-1.0×10^{-3}	-9.3×10^{-4}
Winter, 28 km	-1.6×10^{-2}	-1.8×10^{-2}	-3.7×10^{-4}	-4.1×10^{-4}
Summer 20 km	-6.6×10^{-4}	-1.2×10^{-3}	-5.6×10^{-5}	-9.9×10^{-5}
Summer, 28 km	2.1×10^{-3}	-1.8×10^{-3}	5.1×10^{-5}	-4.5×10^{-5}

See text for variable descriptions.

tum flux of each detected wave packet. We computed the height profiles of momentum flux by assuming a Gaussian shape of the wave packets with a full width at half maximum as determined by the wavelet analysis. We used (2) to compute the momentum flux from values of $\overline{u'\hat{T}'_{+90}}$ calculated from the perturbation amplitudes of the detected wave packets. The density at the height of the wave packet was obtained from monthly averaged temperature profiles using the hydrostatic approximation; that is,

$$\rho(z) = \rho(z_o) \exp^{-\int_{z_o}^{z} \frac{dz'}{H_\rho(z')}}, \tag{3}$$

where

$$H_\rho = \frac{1}{\frac{g}{RT} + \frac{1}{T}\frac{dT}{dz}} \tag{4}$$

is the density scale height.

Figure 1 shows contour plots of monthly averages of $\rho\overline{u'w'}\delta_-$ and $\rho\overline{v'w'}\delta_-$ calculated for all detected waves with intrinsic frequencies less than 10 f. Here f is the Coriolis frequency, which has a value of 1.19 10^{-4} rad s^{-1} at Macquarie Island, corresponding to a period of ~14.7 hours. This cutoff was chosen as the majority of the detected waves have frequencies ¡ 10 f, and the determination of intrinsic frequencies from hodograph analysis is prone to large uncertainties for high intrinsic frequencies. The mean values of the momentum fluxes at heights of 20 and 28 km are given in Table 1 for summer and winter.

The shape of the momentum flux profiles agrees well with *Allen* [1996], although our values are up to an order of magnitude smaller than the ones reported by *Allen* [1996] and *Vincent et al.* [1997]. This, however, can be explained by the restriction of our analysis to waves with intrinsic frequencies ¡ 10 f, while *Allen* [1996] and *Vincent et al.* [1997] used the full spectrum of waves in their calculations. More important, the spectral approach adopted by *Allen* [1996] and *Vincent et al.* [1997] to calculate a mean frequency almost certainly overestimates the wave fluxes [*Vincent and Alexander*, 2000; *Alexander and Vincent*, 2000].

In comparison with other experimental observations and in assessing the importance of the observed gravity waves for the mean circulation, the limited frequency range and our vertical wavelength bandwidth of ~1.2 to 11 km have to be kept in mind. For the same reason an estimation of mean-flow acceleration from these momentum flux profiles is prone to large errors: Consider a wave packet propagating dissipationless through the background atmosphere. Owing to changes in background wind, the vertical wavenumber of the wave packet will change along its path. If the vertical wavenumber is within the observable range for certain height regions and out of this range for other height regions, the momentum flux profile from radiosonde observations will show artificial variations with height, leading to errors in the calculated accelerations of the background wind.

One can circumvent this difficulty if ray-tracing techniques are applied. After extracting the wave parameters in a height region where the wave packet is observable, the parameters of the wave packet can be calculated for the whole height range of interest. It is then possible to compute the momentum flux even for those height regions, where the vertical wavenumber of the wave packet is not within the observable range, avoiding variations in the momentum flux estimates due to the observational filter. Ray tracing, furthermore, enables us to propagate the gravity wave spectrum to higher regions of the atmosphere which are inaccessible to direct measurements with radiosondes.

3. Mean-flow Accelerations and Intermittency

3.1. A Linear Ray-Tracing Model

For our modeling studies we applied a simple, linear-ray tracing model similar to *Eckermann* [1992], *Marks and Eckermann* [1995], *Alexander* [1996], and *Warner and McIntyre* [1996]. A single-column model is adopted, since we have access to data from one geographic location and have no information about the fine-scale "geography" of wave sources [*Warner and McIntyre*, 1996].

If one assumes no explicit dependence of the background atmosphere on horizontal position x and y and time t, then the horizontal wavenumbers k and l and the ground-based frequency ω of a wave packet are constant

along its ray. The intrinsic frequency $\hat{\omega}$ as a function of height is then given by

$$\hat{\omega}(z) = \omega - u(z)k - v(z)l, \tag{5}$$

and the vertical wavenumber $m(z)$ can be obtained from the dispersion relation.

The integration along the ray path is taken from the source level until a turning or critical level is encountered, i.e. $m \to 0$ or $\hat{\omega} \to f$, respectively. In the absence of dissipation, the amplitude of the wave packet along the ray is determined by the conservation of wave action flux [*Lighthill*, 1978], which, in a single-column model, can be written as

$$F = \frac{c_{g,z}E}{\hat{\omega}} = \text{const}, \tag{6}$$

where $c_{g,z}$ is the vertical group velocity and E the total energy density. Using the polarization equations in the Boussinesq approximation, this can be expressed as

$$F = -\frac{1}{2m}\rho \hat{u}_{||}'^2 \left(1 - \frac{f^2}{\hat{\omega}^2}\right) = \text{const}, \tag{7}$$

where $\hat{u}_{||}'$ is the peak perturbation amplitude parallel to the intrinsic propagation direction of the wave packet.

Equation (7) is used to calculate the amplitude of the wave packet from one level to the next when dissipation is negligible. Radiative damping, however, can severely attenuate the amplitude of slowly propagating gravity waves. We therefore included this dissipative process in our model using the parameterization of *Zhu* [1993]. His scheme allows the calculation of the scale-dependent radiative damping rate τ_{rad} as a function of altitude for a given temperature profile. Radiative damping attenuates the amplitude of a wave packet by a factor $\exp(-\tau_{\text{rad}}(z)\Delta z/c_{g,z}(z))$ during its propagation through a height interval Δz at height z. Figure 2 shows examples of damping rates for the COSPAR International Reference Atmosphere (CIRA) in June at 50° S.

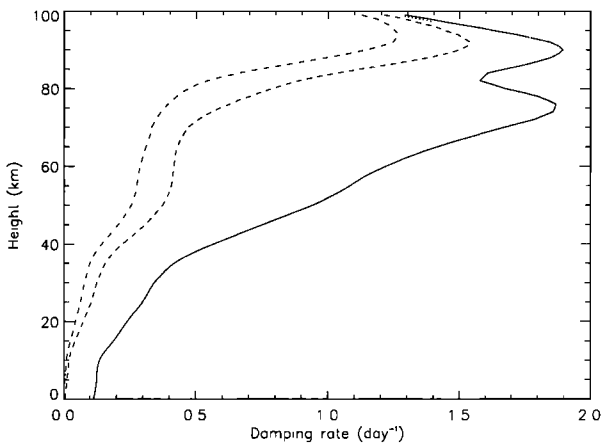

Figure 2. Radiative damping rates for the Cospar International Reference Atmosphere (CIRA) in June at 50° S for vertical wavelengths of 2 (solid curve), 5 (dotted curve), 10 (dashed curve), and 20 (dot-dashed curve) km.

If the resulting amplitude exceeds the critical amplitude for dynamical instability (equation (16) in ZV), it is thresholded to this value. This corresponds to a dissipation mechanism that acts instantaneously once the critical amplitude is reached and stops as soon as the amplitude is restored to a subcritical value. This approach is often used, but it is, of course, not entirely self-consistent since the linear solution will break down before breaking occurs [*Andrews et al.*, 1987]. The existence of a threshold amplitude for instability renders the saturation mechanism nonlinear. Hence it is important to use actual wave packet amplitudes and not averages over space or time.

3.2. Intermittency and Gravity Wave Source Spectrum

While the nonlinear saturation mechanism requires the knowledge of actual wave packet amplitudes to correctly identify the heights where saturation becomes important, the mean zonal acceleration (1) depends on the temporally averaged momentum flux. The observation of wave packets in the radiosonde data indicates a degree of intermittency in the gravity wave field; that is, the wave packets are present only for a certain amount of time at each height level. The observed intermittency may be due to several factors, including intermittency of the sources themselves. Propagation of waves from other latitudes and longitudes, and the associated propagation effects, could also lead to the observed intermittency.

While we make no assumptions about the cause(s) of the intermittency, we do need to quantify the degree of intermittency in order to apply a correction factor to the momentum flux profile of each wave packet to obtain the required temporal average. Owing to the lack of information about wave intermittency, this correction factor was chosen arbitrarily in previous modeling studies to give reasonable magnitudes of acceleration at the required levels in the atmosphere [*Alexander and Rosenlof*, 1996; *Hamilton*, 1997]. The use of wavelet analysis, however, gives us information about the vertical extent of the gravity wave packets and can shed some light on the gravity wave intermittency.

We define the residence time τ of a wave packet as the time it takes to completely traverse an arbitrary height level

$$\tau = \int_{z_{\text{lower}}}^{z_{\text{upper}}} \frac{dz}{c_{g,z}(z)}, \tag{8}$$

where z_{lower} and z_{upper} are the lower and upper boundary, respectively, of the wave packet at the time of detection and $c_{g,z}(z)$ is the vertical group velocity as a function of height. Monthly averaged values of $u(z)$, $v(z)$, and $T(z)$ were used for the calculation of $c_{g,z}(z)$.

It is important to realize that the residence time τ is independent of the chosen height level: Consider an upward propagating wave packet extending from z_{lower} to z_{upper}. It will take the upper end of the wave packet a certain time to reach an arbitrary height level above z_{upper}. The lower end of the wave packet will take the same time plus the time it takes to propagate from z_{lower} to z_{upper}. Thus the wave packet will be present at the arbitrary height level for the residence time τ, independent of the choice of the height level. Any change in group velocity $c_{g,z}$ along the propagation path is compensated by a stretching or shrinking of the wave packet. The residence time is therefore an invariant of the gravity wave propagation and equals the time the gravity wave source was turned on for the generation of the observed wave packet. Note that our definition of the residence time differs from that of *Alexander* [1998], who defined the residence time as the ratio of a constant height interval to vertical group velocity. Her residence time is therefore a function of height, as she did not take the shrinking and stretching of the wave packet into account.

We can then define the intermittency of the wave packet as

$$\epsilon = \frac{\tau}{T_{\max}}, \tag{9}$$

where $T_{\max}$ is the residence time of a hypothetical wave packet extending over all those height regions where it could have been observed with the applied analysis method. $T_{\max}$ can be calculated as

$$T_{\max} = \int_{z_{\min}}^{z_{\max}'} \frac{dz}{c_{g,z}(z)}, \tag{10}$$

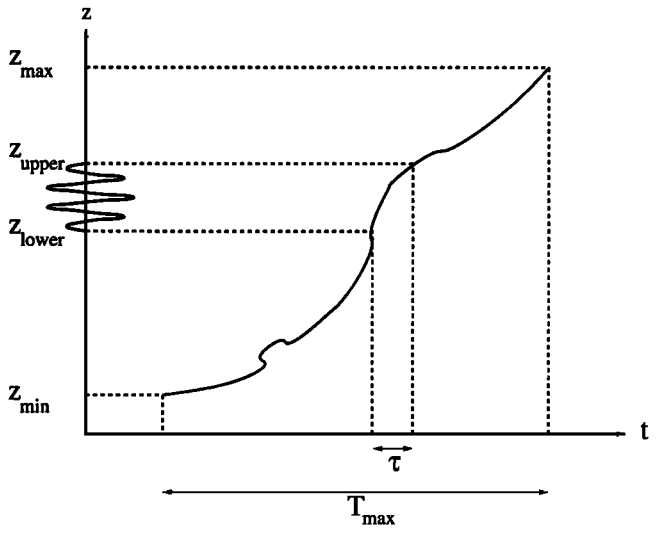

Figure 3. Trajectory of a wave packet observed between boundaries z_{lower} and z_{upper}. The residence time τ is the time the gravity wave source had to be switched on to produce the observed wave packet. If the wave packet extended over the whole observed height interval $[z_{\min}, z_{\max}]$,q the gravity wave source would have had to be active for the whole time $T_{\max}$.

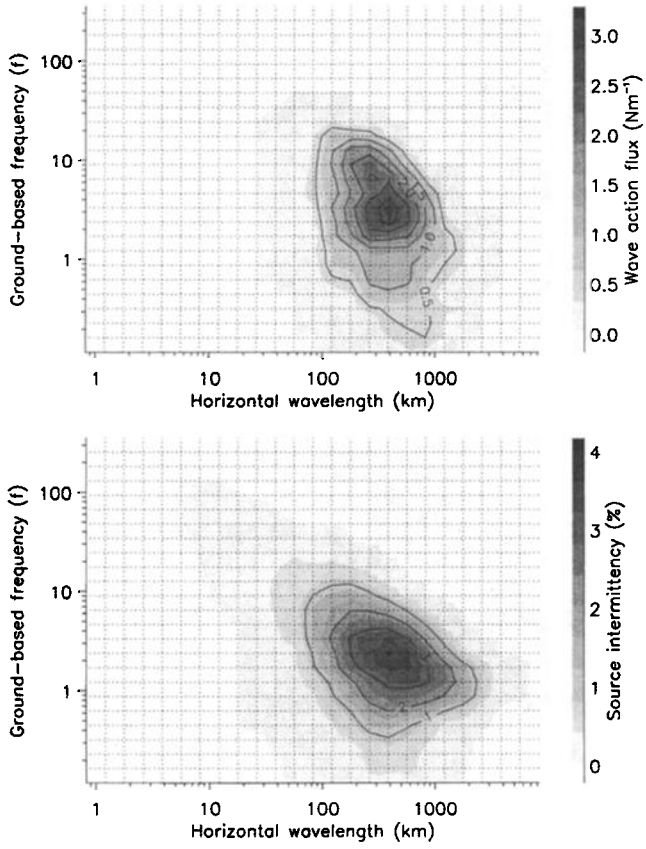

Figure 4. Contour plot of average (top) wave action flux and (bottom) intermittency as a function of horizontal wavelength and ground-based frequency for summer. The dashed lines show the intervals over which the data have been binned.

where the prime indicates integration over only those height intervals where the vertical wavenumber $m(z)$ is within the observable range. The method is illustrated in Figure 3.

The horizontal wavenumber vector $\mathbf{k_h}$, the ground-based frequency ω, the wave action flux F, and the wave intermittency ϵ are all invariants of the dissipationless wave propagation through a horizontally isotropic steady state atmosphere. They fully characterize the wave packet and its effect on the atmosphere in our model. The applied observation method, however, cannot provide information about the full $(\mathbf{k_h}, \omega)$ spectrum. As indicated above, the radiosonde technique can only observe gravity waves with vertical wavelengths between ~1.2 and 11 km. Owing to this observational filter, only certain parts of the $(\mathbf{k_h}, \omega)$ spectrum are observable at each height. Changes in background wind with height Doppler shift different parts of the $(\mathbf{k_h}, \omega)$ spectrum into the observable wavenumber range, so that different parts of the spectrum can be observed at different heights. Because of the invariance of $\mathbf{k_h}$, ω, F, and τ, however, these wave parameters are independent of height and a larger part of the gravity wave spectrum can be reconstructed. By using different ob-

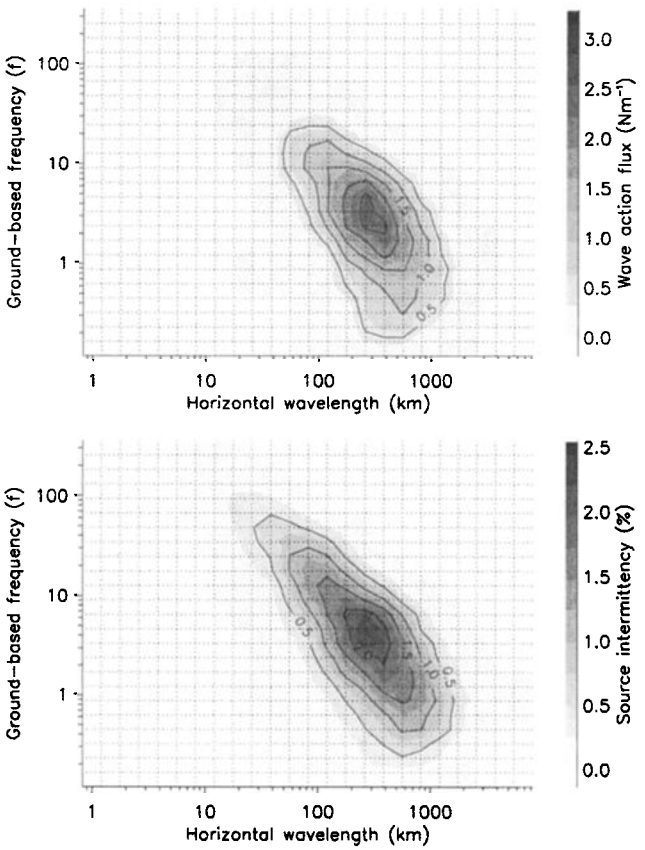

Figure 5. Same as Figure 4, but for winter.

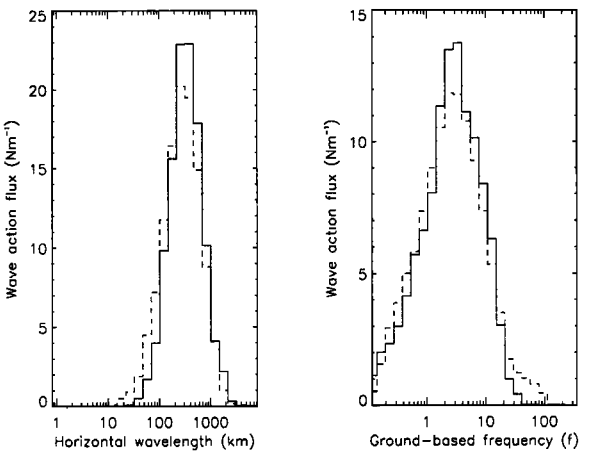

Figure 6. Average wave action flux as a function of (left) horizontal wavelength and (right) ground-based frequency for winter (dashed curve) and summer (solid curve).

servation techniques together, one can obtain more detailed information about the spectrum.

Figures 4 and 5 illustrate the source spectra reconstructed from our observations for summer and winter, respectively. These source spectra correspond to the spectra that, when input at a height of 15 km, will reproduce the observed characteristics of the gravity wave field. It is important to note that, for the reasons given above, it is not necessarily the spectrum emitted by a physical source somewhere in the lower atmosphere. To obtain better statistics, all information about wave propagation directions was discarded in our spectra and only the magnitudes of the horizontal wavenumber vector $\mathbf{k_h}$ and the ground-based frequency ω were utilized. The figures contour plots of time-averaged wave action flux

$$\overline{F}(k_h,\omega) = \frac{1}{N}\sum_{i=1}^{N} \|F(k_h,\omega,i)\| \frac{\tau(k_h,\omega,i)}{T_{\max}(k_h,\omega,i)} \qquad (11)$$

and source intermittency

$$\bar{\epsilon}(k_h,\omega) = \frac{1}{N}\sum_{i=1}^{N} \frac{\tau(k_h,\omega,i)}{T_{\max}(k_h,\omega,i)}, \qquad (12)$$

where i is an index to the different radiosonde soundings, and the data were slightly smoothed with a three-point running mean. The analyzed height range was from 15 km to the maximum height of the soundings, often reaching up to 30 km. The horizontal wavenumber k_h and the ground-based frequency ω were binned logarithmically into 25 bins for the ranges $k_h = 2\pi/10^7\text{m} \ldots 2\pi/10^3\text{m}$ and $\omega = 0.1f \ldots 300f$, respectively.

For a better comparison of source strength between the two seasons, the average source strength is shown as a one-dimensional function of horizontal wavelength and ground-based frequency for winter and summer in Figure 6. It is evident that the total wave action flux in the observed vertical wavenumber range is very similar in magnitude for winter and summer. This corroborates the argument that the differences in horizontal wind variance as presented in ZV (Figure 7) can be largely due to seasonal changes in the background atmosphere. It is also noteworthy that while the gravity wave field was shown in ZV to be clearly dominated by low intrinsic frequency, inertia-gravity waves, the Doppler shifting by the background wind leads to tails

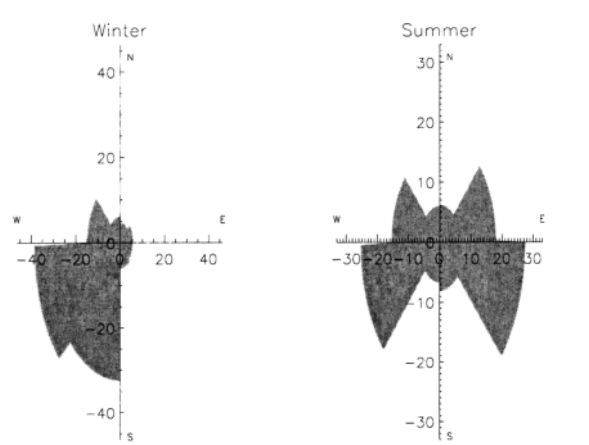

Figure 7. Average wave action flux as a function of intrinsic horizontal propagation direction for (left) winter and (right) summer. Units are N m^{-1}.

in the ground-based frequency distribution to both low and high frequencies. Figure 7 shows the average wave action flux as a function of intrinsic horizontal propagation direction for winter and summer. In both cases the observed wave action flux is distributed anisotropically. This observed anisotropy does not necessarily imply an anisotropic wave field but may, again, be due to the observational filter of the radiosonde method. If the dominant background wind is confined to certain azimuths, then only certain regions of the $(\mathbf{k_h}, \omega)$ spectrum contribute to our observations, and what might be an isotropic wave field can appear anisotropic in observations.

3.3. Mean-flow Accelerations

In our model we ray-traced all upward propagating gravity wave packets detected above 15 km for each month of the year to a maximum height of 100 km. As a starting level we chose the lowest height above $z_{\text{start}} =$ 15 km from where a propagation of a wave packet to its level of detection was possible in the given background atmosphere (Figure 8). We make no assumptions about the origin of the waves. They may have originated at nearby heights through generation by wind shears, for example, or they may have propagated horizontally into the region of observation. Ray-tracing studies of inertia-gravity waves observed at Macquarie Island by *Guest et al.* [2000] show that the waves can propagate several hundred kilometers from tropospheric sources located to the west (upstream) of the island.

The wave action flux of the wave packet at the starting level was adjusted to reach agreement between model and observation at the detection level and to compensate for any radiation damping effects. A height resolution of 500 m was used and no interaction of the packets was allowed. As background atmosphere we used the CIRA 1986 temperature and zonal winds of the respective month linearly interpolated to the required latitude of 55°S. A contour plot of the zonal wind profiles is given in Figure 9. The acceleration was calculated using (1) with

$$\langle \rho u' w' \delta_- \rangle = \epsilon k F \tag{13}$$

computed for each wave packet, with ϵ as the correction factor required to account for the temporal average.

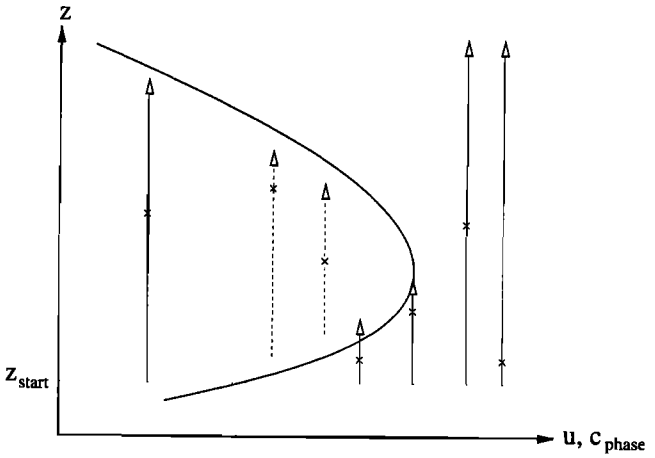

Figure 8. Starting level for each wave packet, chosen as the lowest height above z_{start} from where a propagation of the wave packet to its level of detection (crosses) was possible. Wave propagation from a uniform starting level z_{start} could not reproduce the effects of waves observed above a possible critical level (dashed lines).

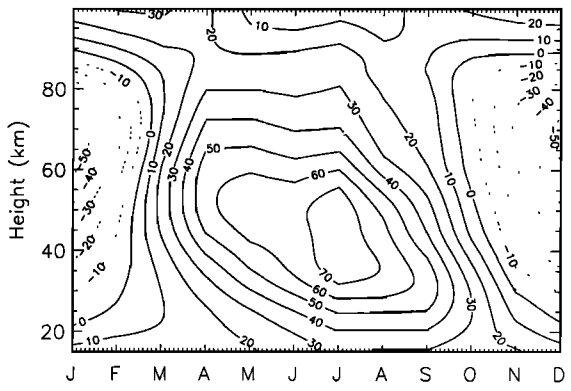

Figure 9. CIRA zonal winds (m s^{-1}) linearly interpolated to 55°S.

Figure 10 shows a contour plot of the inferred zonal accelerations in the mesosphere. The accelerations are most significant at regions of high wind shear, at around 85 km during summer and between 60 and 80 km during winter. The magnitude of the wave drag in winter seems to be about 2 to 3 times higher than the average drag expected both from observations and theory [*Fritts and Vincent*, 1987; *Fritts and Yuan*, 1989; *Holton*, 1983]. The accelerations deduced from our model, however, are based on the data from a single station only and might deviate from a zonal average over all longitudes.

In contrast to the decelarative effect of the waves in the mesosphere, our model reveals an accelerative effect in the middle stratosphere (Figure 11). This is in agreement with calculations of *Alexander and Rosenlof* [1996], who used global measurements of temperature,

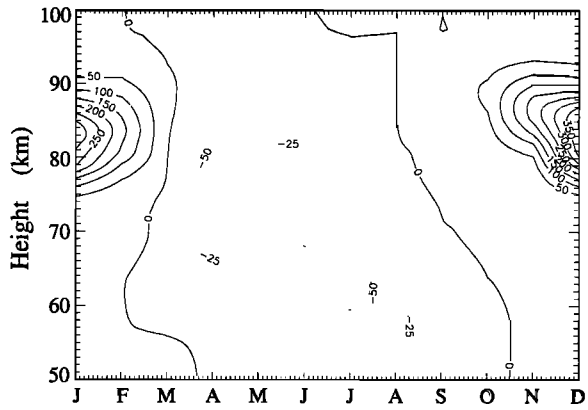

Figure 10. Inferred zonal accelerations (m s^{-1} d^{-1}) in the mesosphere. Solid contour lines correspond to eastward acceleration.

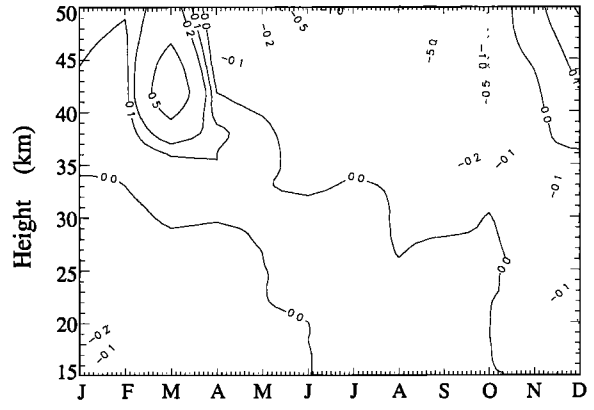

Figure 11. Same as Figure 10, but for the stratosphere.

wind, and chemical constituents to estimate the zonal mean forcing by unresolved waves in the stratosphere.

It is important to realize that the analysis of the radiosonde data might be biased toward low intrinsic frequency waves, as these waves usually have larger amplitudes than their high-frequency counterparts and are thus easier to detect. Waves of high intrinsic frequency, while smaller in amplitude, might still outweigh the effect of the observed low-frequency waves. Nevertheless, our computations show that waves with low intrinsic frequency in the stratosphere can have a profound impact on the circulation in the middle atmosphere, at least in our simple linear model.

4. Summary and Conclusions

We used the wave parameters of gravity wave packets detected in the lower stratosphere over Macquarie Island to assess the influence of the observed gravity wave field on the mean flow. While a direct computation of a vertical momentum flux profile corresponding to the wave packets observed at the respective heights is possible, the observational filter of the radiosonde technique, together with the Doppler shifting of the wave packets due to a height-variable background atmosphere, prohibit the determination of mean-flow accelerations from these profiles.

To overcome this problem, we input the detected waves in a linear ray-tracing model from a common source level. The calculation of a momentum flux profile is then possible even at those heights, where the wave packets would be outside the observationally accessible vertical wavenumber range. The definition of a wave source intermittency then allows the calculation of a temporally averaged momentum flux profile for each detected wave packet.

The inferred mean-flow decelerations in the mesosphere were shown to be up to a factor of 2 to 3 times higher than measurements and theory would predict. In the lower stratosphere the waves lead to an acceleration of the mean flow in accordance with theoretical predictions.

In conclusion, it should be emphasized that there are a number of limitations to our approach. First, the observational filtering inherent in the radiosonde measurements means that only part of the wave spectrum is included. High phase speed, long vertical wavelength waves are not observed, so that our results pertain to low-frequncy inertia-gravity waves. Second, for reasons of computational efficiency and lack of information on the gravity wave field at other latitudes, we adopt a single-column approach and neglect meridional propagation. This is not to say that drag due to meriodionally propagating gravity waves may be not be important [e.g., *Lieberman*, 1999]. Within these limitations, however, our results show that lower stratospheric inertia-gravity waves can significantly influence the momentum budget of the upper middle atmosphere, contrary to what is sometimes assumed.

Acknowledgments. The authors would like to thank Joan Alexander for corrections and comments to an earlier version of this manuscript. We acknowledge the provision of the radiosonde data by the Australian Bureau of Meteorology.

References

Alexander, M. J., A simulated spectrum of convectively generated gravity waves: Propagation from the tropopause to the mesopause and effects on the middle atmosphere, *J. Geophys. Res.*, *101*, 1571–1588, 1996.

Alexander, M. J., Interpretations of observed climatological patterns in stratospheric gravity wave variance, *J. Geophys. Res.*, *103*, 8627–8640, 1998.

Alexander, M. J., and L. Pfister, Gravity wave momentum flux in the lower stratosphere over convection, *Geophys. Res. Lett.*, *22*, 2029–2032, 1995.

Alexander, M. J., and K. H. Rosenlof, Nonstationary gravity wave forcing of the stratospheric zonal mean wind, *J. Geophys. Res.*, *101*, 23,465–23,474, 1996.

Alexander, M. J., and R. A. Vincent, Gravity waves in the tropical lower stratosphere: A model study of seasonal and interannual variability, *J. Geophys. Res.*, *105*, 17,983–17,993, 2000.

Allen, S. J., Gravity wave motions in the troposphere and lower stratosphere, Ph.D. thesis, Univ. of Adelaide, Adelaide, South Aust., 1996.

Andrews, D. G., J. R. Holton, and C. B.Leovy, *Middle Atmosphere Dynamics*, Academic, San Diego, Calif., 1987.

Dunkerton, T. J., Theory of the mesopause semiannual oscillation, *J. Atmos. Sci.*, *39*, 2681–2690, 1982.

Eckermann, S. D., Ray-tracing simulation of the global propagation of inertia gravity waves through the zonally averaged middle atmosphere, *J. Geophys. Res.*, *97*, 15,849–15,866, 1992.

Fritts, D. C., Gravity wave saturation in the middle atmosphere: A review of theory and observations, *Rev. Geophys.*, *22*, 275–308, 1984.

Fritts, D. C., and T. E. VanZandt, Spectral estimates of gravity wave energy and momentum fluxes, i, Energy dissipation, acceleration and constraints, *J. Atmos. Sci.*, *50*, 3685–3694, 1993.

Fritts, D. C., and R. A. Vincent, Mesospheric momentum flux studies at Adelaide, Australia: Observations and a gravity wave-tidal interaction model, *J. Atmos. Sci.*, *44*, 605–619, 1987.

Fritts, D. C., and L. Yuan, Measurement of momentum

fluxes near the summer mesopause at Poker Flat, Alaska, *J. Atmos. Sci.*, *46*, 2569–2579, 1989.

Fritts, D. C., T. Tsuda, T. E. VanZandt, S. A. Smith, T. Sato, S. Fukao, and S. Kato, Studies of velocity fluctuations in the lower atmosphere using the MU radar, II, Momentum fluxes and energy densities, *J. Atmos. Sci.*, *47*, 51–66, 1990.

Garcia, R. R., and S. Solomon, The effect of breaking gravity waves on the dynamics and chemical composition of the mesosphere and lower thermosphere, *J. Geophys. Res.*, *90*, 3850–3860, 1985.

Geller, M. A., Dynamics of the middle atmosphere, *Space Sci. Rev.*, *34*, 359–375, 1983.

Guest, F. M., M. J. Reeder, C. J. Marks, and D. J. Karoly, Inertia-gravity waves observed in the lower stratosphere over Macquarie Island, *J. Atmos. Sci.*, *57*, 737–752, 2000.

Hamilton, K., The role of parameterized drag in a troposphere-stratosphere-mesosphere general circulation model, in *Gravity Wave Processes: Their Parametrization in Global Climate Models*, edited by K. Hamilton, pp. 337–350, Springer-Verlag, New York, 1997.

Hines, C. O., Doppler-spread parametrization of gravity-wave momentum deposition in the middle atmosphere, 1, Basic formulation, *J. Atmos. Sol. Terr. Phys.*, *59*, 371–386, 1997.

Holton, J. R., The role of gravity wave induced drag and diffusion in the momentum budget of the mesosphere, *J. Atmos. Sci.*, *39*, 791–799, 1982.

Holton, J. R., The influence of gravity wave breaking on the general circulation of the middle atmosphere, *J. Atmos. Sci.*, *40*, 2497–2507, 1983.

Lieberman, R. S., The gradient wind in the mesosphere and lower thermosphere, *Earth Planets Space*, *51*, 751–761, 1999.

Lighthill, J., *Waves in Fluids*, Cambridge Univ. Press, New York, 1978.

Lilly, D. K., and P. J. Kennedy, Observations of a stationary mountain wave and its associated momentum flux and energy dissipation, *J. Atmos. Sci.*, *30*, 1135–1152, 1973.

Lindzen, R. S., Turbulence and stress owing to gravity wave and tidal breakdown, *J. Geophys. Res.*, *86*, 9707–9714, 1981.

Marks, C. J., and S. D. Eckermann, A three-dimensional nonhydrostatic ray-tracing model for gravity waves: Formulation and preliminary results for the middle atmosphere, *J. Atmos. Sci.*, *52*, 1959–1984, 1995.

Mobbs, S. D., and J. M. Rees, Studies of atmospheric internal gravity waves at Halley station, Antarctica, using radiosondes, *Antarct. Sci.*, *1*, 65–75, 1989.

Murayama, Y., T. Tsuda, and S. Fukao, Seasonal variation of gravity wave activity in the lower atmosphere observed with the MU radar, *J. Geophys. Res.*, *99*, 23,057–23,069, 1994.

Reid, I. M., and R. A. Vincent, Measurements of mesospheric gravity wave momentum fluxes and mean flow accelerations at Adelaide, Australia, *J. Atmos. Sol. Terr. Phys.*, *49*, 443–460, 1987.

Sato, K., A statistical study of the structure, saturation and sources of inertio-gravity waves in the lower stratosphere observed with the MU radar, *J. Atmos. Sol. Terr. Phys.*, *56*, 755–774, 1994.

Sato, K., and T. J. Dunkerton, Estimates of momentum flux associated with equatorial Kelvin and gravity waves, *J. Geophys. Res.*, *102*, 26,247–26,261, 1997.

Shutts, G. J., M. Kitchen, and P. H. Hoare, A large amplitude gravity wave in the lower stratosphere detected by radiosonde, *Q. J. R. Meteorol. Soc.*, *114*, 579–594, 1988.

Tsuda, T. S., S. Kato, T. Yokoi, T. Inoue, M. Yamamoto, T. E. VanZandt, S. Fukao, and T. Sato, Gravity waves in the mesosphere observed with the middle and upper atmosphere radar, *Radio Sci.*, *25*, 1005–1018, 1990.

Vincent, R. A., and M. J. Alexander, Gravity waves in the tropical lower stratosphere: An observational study of seasonal and interannual variability, *J. Geophys. Res.*, *105*, 17,971–17,982, 2000.

Vincent, R. A., and I. M. Reid, HF Doppler measurements of mesospheric gravity wave momentum fluxes, *J. Atmos. Sci.*, *40*, 1321–1333, 1983.

Vincent, R. A., S. J. Allen, and S. D. Eckermann, Gravity-wave parameters in the lower stratosphere, in *Gravity Wave Processes: Their Parametrization in Global Climate Models*, edited by K. Hamilton, pp. 7–25, Springer-Verlag, New York, 1997.

Warner, C. D., and M. E. McIntyre, On the propagation and dissipation of gravity wave spectra through a realistic middle atmosphere, *J. Atmos. Sci.*, *53*, 3213–3225, 1996.

Warner, C. D., and M. E. McIntyre, Toward an ultra-simple spectral gravity wave parameterization for general circulation models, *Earth Planets Space*, *51*, 475–484, 1999.

Worthington, R. M., and L. Thomas, The measurement of gravity wave momentum flux in the lower atmosphere using VHF radar, *Radio Sci.*, *31*, 1501–1517, 1996.

Zhu, X., Radiative damping revisited: Parameterization of damping rate in the middle atmosphere, *J. Atmos. Sci.*, *50*, 3008–3021, 1993.

Zink, F., and R. A. Vincent, Wavelet analysis of stratospheric gravity wave packets over Macquarie Island, 1. Wave parameters, *J. Geophys. Res.*, this issue.

R. A. Vincent and F. Zink, Department of Physics and Mathematical Physics, University of Adelaide, Adelaide 5005, Australia. (robert.vincent@adelaide.edu.au; fzink@physics.adelaide.edu.au)

(Received January 13, 2000; revised November 2, 2000; accepted November 14, 2000.)